

Chargaff's second parity rule and the kinetics of DNA replication

Pierre Gaspard

*Center for Nonlinear Phenomena and Complex Systems,
Université Libre de Bruxelles (ULB), Code Postal 231, Campus Plaine, B-1050 Brussels, Belgium*

A model of DNA replication is investigated, which is based on the biochemical kinetics of DNA polymerases, copying a DNA strand into its complement, except for rare point-like mutations due to nucleotide substitutions. Numerical simulations of many successive replications starting from an initial DNA sequence show that the fractions of mono- and oligonucleotides converge toward compliance with Chargaff's second parity rule. The theory of this multireplication process reveals that the approximate equalities between the fractions of complementary nucleotides are the consequence of (1) the dominant role of complementarity in the DNA replication kinetic process and (2) the smallness of the polymerase error probability. These two features lead to a robust mechanism underlying Chargaff's second parity rule.

I. INTRODUCTION

The genome of organisms is encoded in deoxyribonucleic acids (DNA) forming copolymeric sequences of nucleotides linked together by phosphodiester bonds [1]. The four types of nucleotides contain the bases adenine, cytosine, guanine, and thymine, which are more shortly denoted A, C, G, and T, respectively. Discovered in 1950, Chargaff's first parity rule states that the fractions of complementary nucleotides are equal in DNA, $A = T$ and $C = G$ [2–5]. This rule is the direct consequence of complementary base pairing, A:T and C:G, by hydrogen bonds between the two strands of DNA. The equalities $A = T$ and $C = G$ of Chargaff's first parity rule are thus explained by the interstrand symmetry due to the double helix structure of DNA, established by Watson and Crick in 1953 [6, 7].

Discovered in 1968, Chargaff's second parity rule stipulates the approximate equalities $A \simeq T$ and $C \simeq G$ between the fractions of complementary nucleotides in each one of the two strands of DNA [8, 9]. Furthermore, it was discovered that Chargaff's second parity rule extends to the fractions of complementary oligonucleotides in each single strand of DNA [10–13]. Today, Chargaff's second parity rule is observed in most genomes: those of bacteria, archaea, eukaryota, and double-stranded DNA viruses. Deviations with respect to this rule exist for the genomes of mammalian mitochondria and single-stranded DNA or RNA viruses [14, 15].

Many hypotheses have been formulated in order to understand the origins of Chargaff's second parity rule. The issue is that this approximate intrastrand symmetry cannot be explained by the double helix structure of DNA, as for Chargaff's first parity rule. Nevertheless, it is understood that the composition of each one of the two DNA strands is the result of an evolutionary process spanning over many replications, during which mutations have occurred. In this respect, mathematical models have been proposed for the evolution of mononucleotide fractions under the mutational pressure of nucleotide substitutions. In particular, under the hypothesis of no-strand-bias conditions for the substitution rates, there is convergence toward strict equalities between the fractions of complementary nucleotides [16, 17]. This model can be generalized to allow a stochastic evolution toward approximately equal fractions with suitable fitting to experimental data [18–20]. If such models can describe the evolution of nucleotide fractions, they do not provide an understanding for the origins of the phenomenon.

Furthermore, several mechanisms have been considered to explain Chargaff's second parity rule. In particular, it has been assumed that the presence of complementary oligonucleotides in DNA sequences could provide an evolutionary advantage by increasing the potential to form stem-loops [21–23]. Mechanisms have also been considered that are based on mutations by inversions and inverted transpositions [24, 25] or by inversions only [26]. In the last two mechanisms, the fractions of complementary nucleotides converge during evolution toward values compliant with Chargaff's second parity rule, while preserving their mean initial values, i.e., $\lim_{r \rightarrow \infty} A_r = \lim_{r \rightarrow \infty} T_r = (A_0 + T_0)/2$ and $\lim_{r \rightarrow \infty} C_r = \lim_{r \rightarrow \infty} G_r = (C_0 + G_0)/2$, featuring a role to primordial genome, although these mean values are observed to be specific to each species. The causes of Chargaff's second parity rule thus remain elusive.

Here, our purpose is to revisit studies of successive DNA replications based on detailed kinetic models for DNA polymerases, where numerical evidence was obtained for the maintain of approximate equalities between the fractions of complementary nucleotides [27, 28]. These numerical simulations gave a hint that many successive DNA replications may lead to compliance with Chargaff's second parity rule. However, the sole polymerase used in Refs. [27, 28] is the human mitochondrial DNA polymerase γ , which is not representative of typical polymerases acting for the replication (or the repair) of the main genome of organisms. Therefore, we here consider more typical DNA polymerases, namely, the polymerases Dpo1 [29], Dpo3 [30], and Dpo4 [31] from the archaeon *Sulfolobus solfataricus* P2, the D-family DNA polymerase from *Thermococcus* archaeon species 9°N [32], and the wild-type rat DNA polymerase β [33]. The polymerization rate constants and the dissociation constants of these polymerases have been measured experimentally

with pre-steady-state kinetic methods. The knowledge of these constants can be used for the numerical simulation of many successive replications, starting from arbitrary initial templates. At each replication, the simulation proceeds by stochastic events generated with Gillespie's kinetic Monte Carlo algorithm [34, 35], attaching or detaching a nucleotide to the end of the copy growing along a template. This process is repeated many successive times. The fractions of mono- and oligonucleotides are numerically measured in each copy in order to determine their evolution with the number of replications and to test the validity of Chargaff's second parity rule.

After this introduction, the paper is organized as follows. In Sections II and III, we consider the case where the kinetics of DNA polymerases do not depend on the previously incorporated nucleotide. Section II presents the results of numerical simulations for the five DNA polymerases here considered. Section III is devoted to the theory of the simulations, showing that the nucleotide fractions converge toward asymptotic values complying with Chargaff's second parity rule in the sense that, asymptotically, the fractions of complementary nucleotides are approximately equal to each other up to unequal corrections of the order of the polymerase error probability. In Section IV, the study is extended to polymerase kinetics with a dependence on the previously incorporated nucleotide, confirming the convergence toward compliance with Chargaff's second parity rule. Conclusion and perspectives are drawn in Section V.

II. SIMULATION OF MANY SUCCESSIVE DNA REPLICATIONS

A. Model of successive DNA replication

We consider a model where many DNA replications are successively performed by some type of polymerase. Every replication is a template-directed copolymerization process generating a new DNA strand from the previous one, as schematically represented in Fig. 1. Every DNA strand is a chain of monomeric units, which are the deoxyribonucleotides A, C, G, or T. The polymerase always moves from the 3' chain end of the template toward its 5' chain end. The copy is synthesized from its 5' to its 3' chain end.

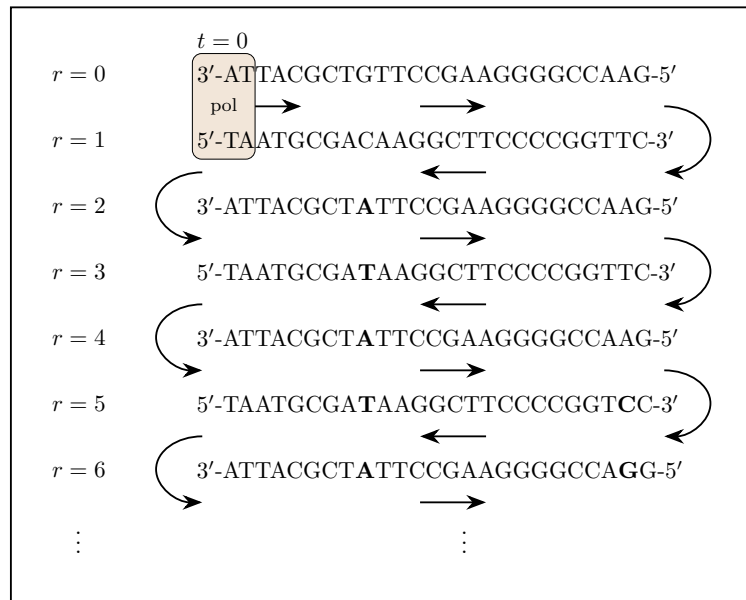
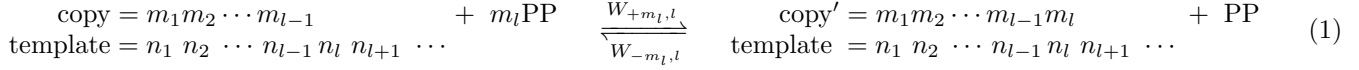


FIG. 1: Schematic representation of many successive DNA replications $r = 1, 2, 3, \dots$. Some DNA polymerase (pol) is depicted at time $t = 0$ at the beginning of the replication of the template $r = 0$ into its copy $r = 1$, which is further replicated into the copies $r = 2, 3, \dots$. Every replication proceeds from the 3' to the 5' chain end of the template, hence the zigzag progress of the successive replications. Replication errors may happen substituting a few nucleotides into non-complementary ones (in bold). The successive replications may be achieved by several DNA polymerases of the same type.

Every replication of a template sequence into a copy sequence is generated by random events attaching (and possibly detaching) nucleotides to the copy under the catalytic action of the polymerase according to the following reaction

scheme:



where $m_j \in \{\text{A, C, G, T}\}$ denotes the j^{th} nucleotide in the copy and $n_j \in \{\text{A, C, G, T}\}$ the j^{th} nucleotide in the template. Prior to its incorporation as a deoxyribonucleoside monophosphate into the copy, the unit m_l was in the intracellular aqueous solution in the form $m_l \text{PP}$ of a deoxyribonucleoside triphosphate dATP, dCTP, dGTP, or dTTP. Upon its binding to the copy, a pyrophosphate PP is released into the solution.

The attachment and detachment rates are denoted $W_{\pm m_l, l}$, respectively. They depend on the intracellular concentrations of dATP, dCTP, dGTP, and dTTP at the time of the replication. The copy grows if the nucleotide concentrations are high enough for the attachment rates $W_{+m_l, l}$ to be sufficiently larger than the detachment rates $W_{-m_l, l}$. As for many other enzymes [36, 38, 39], the dependence of the rates on the concentrations is determined by the Michaelis-Menten kinetics of DNA polymerases, which basically proceeds in two steps. The first step is the rapid binding and unbinding of the nucleoside triphosphate $m_l \text{PP}$ to the template unit n_l by hydrogen bonds, which step is at quasi-equilibrium with Michaelis-Menten constant $K_{m_l}^{n_l}$. The second step is the slower formation of the phosphodiester bond itself with the polymerization rate constant $k_{+m_l}^p$. These constants characterize the kinetics of each type of polymerases and they can be measured experimentally [40]. Table I gives the values of these constants for several types of polymerases.

TABLE I: Kinetic parameters for the exonuclease-deficient DNA polymerases of this study: the DNA polymerases Dpo1 [29], Dpo3 [30], and Dpo4 [31] from *Sulfolobus solfataricus* P2, the D-family DNA polymerase from *Thermococcus* archaeon species 9°N [32], and the wild-type rat DNA polymerase β [33]. These parameters have been measured experimentally using pre-steady-state kinetic methods. k_{+m}^p denotes the polymerization rate constant for the incorporation of the copy nucleotide m paired with the template nucleotide n and K_m^n is the dissociation constant of the pair $m:n$.

	<i>Sulf. solf.</i> Dpo1		<i>Sulf. solf.</i> Dpo3		<i>Sulf. solf.</i> Dpo4		<i>Therm.</i> sp. polD		WT rat pol β	
$m:n$ pair	k_{+m}^p (s^{-1})	K_m^n (μM)								
A:T	11.5	4.9	0.12	18	16.1	206	2.6	2.5	24.1	52
A:G	0.7	2633	0.0025	1900	0.009	334	0.12	320	0.0162	210
A:C	0.34	2300	0.00065	740	0.016	617	1.3	570	0.025	890
A:A	1.3	2800	0.0010	230	0.006	578	0.15	390	0.006	290
C:T	0.7	3300	0.0009	790	0.026	309	0.35	530	0.18	630
C:G	5.7	8.2	0.045	61	7.6	70	3.1	1.7	9.4	8.6
C:C	0.009	2000	0.0015	813.27	0.034	192	0.42	390	0.012	580
C:A	0.7	2633	0.0016	2000	0.013	1036	0.22	450	0.020	200
G:T	0.9	3200	0.0025	410	0.066	935	0.11	300	0.13	850
G:G	0.032	900	0.0021	690	0.008	131	0.07	320	0.0073	230
G:C	5.3	4.1	0.069	24	9.4	171	2.1	0.9	13.5	108
G:A	0.05	1200	0.0017	1700	0.007	1150	0.18	330	0.0079	980
T:T	1.7	4500	0.0015	390	0.034	1941	0.28	490	0.0085	820
T:G	1.3	3500	0.0016	300	0.077	1283	0.38	650	0.11	380
T:C	0.7	2633	0.0013	430	0.011	913	0.55	1400	0.018	2000
T:A	8.2	11	0.038	57	9.4	230	1.8	1.6	16.7	41

The fact is that polymerases may catalyze not only the formation of the four Watson-Crick complementary base pairs, but also that of twelve non-complementary base pairs, leading to point-like nucleotide substitutions in the genome. The attachment rates of the incorrect pairs are significantly smaller than for the correct pairs. Therefore, polymerases generate replication errors with a rate, which defines the error probability η of the polymerase. For the purpose of the present demonstration, we here consider polymerases, which are devoid of exonuclease proofreading activity, so that their error probability is in the range $\eta \sim 10^{-4}\text{-}10^{-3}$. Similar considerations apply to DNA

polymerases having their exonuclease activity, which may decrease their error probability, as discussed here below in Subsection IV C.

The attachment and detachment rates $W_{\pm m_l, l}$ depend not only on the nucleotide m_l that is incorporated, but also on the other molecular groups constituting its environment upon its binding to the copy. These molecular groups include the template nucleotide n_l , with which the base pair $m_l : n_l$ is formed, the neighboring template nucleotides n_{l+1} and n_{l-1} , and possibly also the nucleotide m_{l-1} , which has been previously incorporated into the copy. In the present Section II, we consider the simplest model where the rates do not depend on the previously formed base pair $m_{l-1} : n_{l-1}$. The analytic expressions of the rates of this model are given in Appendix A. In this case, the sequence of the growing copy forms a Bernoulli chain [27, 41, 42]. The more complicated case, where the rates also depend on the previously formed base pair $m_{l-1} : n_{l-1}$, will be considered in Section IV.

The replication of a template into its copy can be numerically simulated with the Gillespie algorithm [34, 35]. Such a replication can be repeated many successive times. Each replication starts again from the 3' chain end of the DNA strand, as shown in Fig. 1. In every successive copy, the fractions of mononucleotides and oligonucleotides are numerically evaluated in order to plot these fractions as functions of the replication number r . These numerical simulations have been carried out for the five polymerases of Table I. The error probability η_r of the r^{th} replication is defined as the fraction of non-complementary (i.e., incorrect) base pairs between the sequences of the copy and the template in the replication. Its asymptotic value η is obtained in the limit $r \rightarrow \infty$.

The numerical simulations of successive replications have been carried out for the three following sets of nucleotide concentrations:

$$\text{concentrations I : } [\text{dATP}] = 3.2 \mu\text{M}, \quad [\text{dCTP}] = 2.1 \mu\text{M}, \quad [\text{dGTP}] = 1.5 \mu\text{M}, \quad [\text{dTTP}] = 5.4 \mu\text{M}; \quad (2)$$

$$\text{concentrations II : } [\text{dATP}] = 24 \mu\text{M}, \quad [\text{dCTP}] = 29 \mu\text{M}, \quad [\text{dGTP}] = 5.2 \mu\text{M}, \quad [\text{dTTP}] = 37 \mu\text{M}; \quad (3)$$

$$\text{concentrations III : } [\text{dATP}] = [\text{dCTP}] = [\text{dGTP}] = [\text{dTTP}] = 100 \mu\text{M}. \quad (4)$$

The concentrations I is the set of mean physiological nucleotide concentrations in normal resting cells and the concentrations II are those in dividing cells [43]. We note that these concentrations are significantly larger than their chemical equilibrium values, which are of the order of nanomolars in the range of 10^{-8} - 10^{-10} M, and where the growth of the copy stops.

TABLE II: Asymptotic values of the nucleotide fractions and the corresponding error probability η for the numerical simulations with Gillespie's algorithm of many successive DNA replications with the exonuclease-deficient DNA polymerases considered in this study: the DNA polymerases Dpo1, Dpo3, and Dpo4 from *Sulfolobus solfataricus* P2, the D-family DNA polymerase from *Thermococcus* archaeon species 9°N, and the wild-type rat DNA polymerase β . In every case, the initial template sequence has equal fractions of nucleotides. The concentrations I-III are given by Eqs. (2)-(4). The statistical errors are smaller than the last digit shown.

DNA polymerase	concentrations	$A(\%)$	$T(\%)$	$C(\%)$	$G(\%)$	η
<i>Sulf. solf.</i> Dpo1	I	45.8	45.8	4.2	4.2	0.00054
	II	43.8	43.8	6.2	6.2	0.00066
	III	33.2	33.2	16.8	16.8	0.00069
<i>Sulf. solf.</i> Dpo3	I	47.4	47.3	2.6	2.7	0.0037
	II	46.4	46.2	3.7	3.7	0.0040
	III	36.7	36.5	13.3	13.5	0.0060
<i>Sulf. solf.</i> Dpo4	I	36.6	36.6	13.4	13.4	0.0019
	II	36.1	36.2	14.0	13.7	0.0040
	III	19.0	19.0	31.0	31.0	0.0022
<i>Therm.</i> sp. polD	I	40.6	40.6	9.4	9.4	0.0012
	II	41.7	41.7	8.3	8.3	0.0017
	III	23.4	23.4	26.6	26.6	0.0013
WT rat pol β	I	34.8	34.8	15.2	15.2	0.00053
	II	32.9	32.9	17.1	17.1	0.00085
	III	17.2	17.2	32.8	32.8	0.00049

Simulations have been performed for the following polymerases.

B. *Sulfolobus solfataricus* P2 DNA polymerase Dpo1

This B-family polymerase carries out the replication of DNA in the hyperthermophilic archaeon *Sulfolobus solfataricus* P2 [29]. The genome of this species contains about 3×10^6 base pairs and its nucleotide fractions are $A \simeq T \simeq 32\%$ and $C \simeq G \simeq 18\%$. The constants of this polymerase have been experimentally measured using pre-steady-state kinetic methods except for three incorrect base pairs, for which typical mean values have been here assumed (see Table I).

The numerical simulation starts from an initial nucleotide template sequence, which is generated as a Bernoulli random chain of length $L = 10^6$ with given fractions A_0 , C_0 , G_0 , and T_0 for the four nucleotides. Its replication is numerically simulated using the Gillespie algorithm, which yields a copy given by a new nucleotide sequence. Next, this new sequence is used as a template for a following replication. This process is repeated over and over again. At each replication r , the content of the sequence is characterized by the fractions of mononucleotides A, C, G, and T; and oligonucleotides AT, TA, AC, GT, ATA, TAT, CTA, and TAG; for the purpose of testing Chargaff's second parity rule.

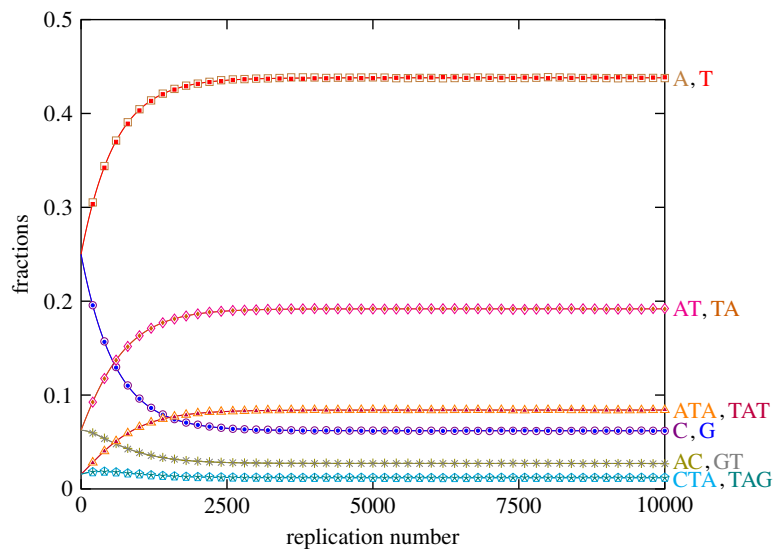


FIG. 2: Fractions of the mononucleotides A (open squares), T (filled squares), C (open circles), G (filled circles), binucleotides AT (open diamonds), TA (filled diamonds), AC (pluses), GT (times), and trinucleotides ATA (open triangles), TAT (filled triangles), CTA (open pentagons), TAG (stars), versus the even values of the replication number r in DNA strands generated by the DNA polymerase Dpo1 from the archaeon *Sulfolobus solfataricus* P2 in a solution with the nucleotide concentrations (3). The initial DNA strand has equal mononucleotide fractions $A_0 = C_0 = G_0 = T_0 = 25\%$. The data points showing the results of the numerical simulation with Gillespie's algorithm are plotted every 200 replications. The solid lines depict the fractions predicted by theory. The asymptotic values of the fractions are given by $A = T = 43.8\%$, $C = G = 6.2\%$, $AT = TA = 19.2\%$, $AC = GT = 2.7\%$, $ATA = TAT = 8.4\%$, and $CTA = TAG = 1.2\%$, as obtained by averaging their values between the replications $r = 9900$ and $r = 10000$.

With the nucleotide concentrations (3), the fractions are shown in Fig. 2 for a simulation starting from an initial template sequence with equal nucleotide fractions $A_0 = C_0 = G_0 = T_0 = 25\%$ and in Fig. 3 for a simulation starting from an initial sequence with unequal nucleotide fractions $A_0 = 70\%$, $C_0 = 15\%$, $G_0 = 10\%$, and $T_0 = 5\%$. Most remarkably, we observe in both cases that the fractions converge toward values that are compliant with Chargaff's second parity rule. Moreover, the fractions have precisely the same asymptotic values independently of the initial nucleotide sequence, as observed in Figs. 2 and 3. These asymptotic values are reported in Table II, together with the corresponding error probability η . The reported values are obtained by averaging over the values between the replications $r = 9900$ and $r = 10000$. We see in Fig. 2 that the convergence to the asymptotic values happens after a number of replications of the order of the inverse η^{-1} of the error probability (which is known as the fidelity of the polymerase). However, in Fig. 3, the convergence to compliant values occurs over a somehow longer number of replications, which will be explained in the next Section III. Simulations have also been carried out for the two other sets of nucleotide concentrations (2) and (4). As seen in Table II, the asymptotic values of the four nucleotides are again compliant with Chargaff's second parity rule. The results also show that the asymptotic values of the nucleotide fractions depend on the intracellular nucleotide concentrations, which is expected since the reaction rates change with

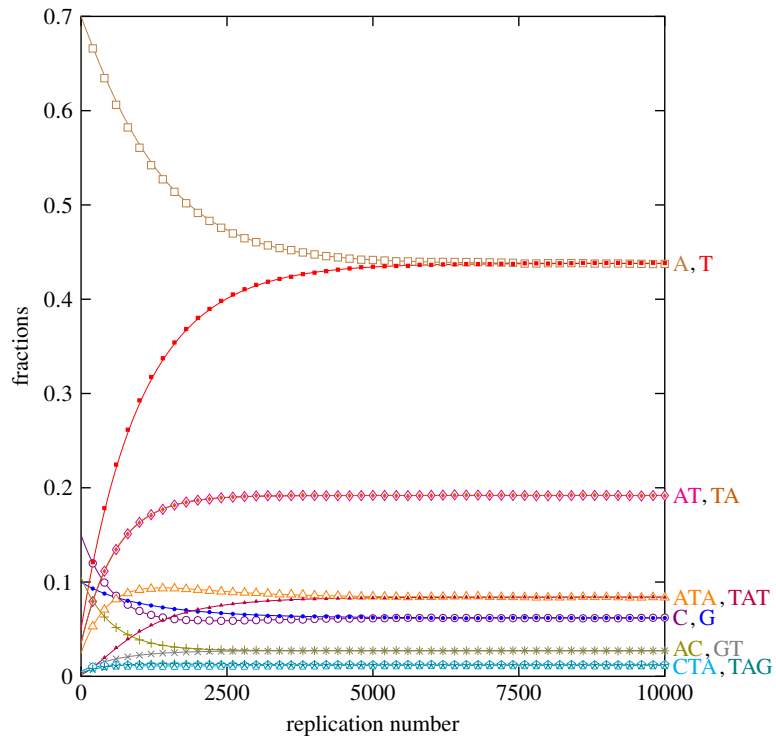


FIG. 3: Fractions of the mononucleotides A (open squares), T (filled squares), C (open circles), G (filled circles), binucleotides AT (open diamonds), TA (filled diamonds), AC (pluses), GT (times), and trinucleotides ATA (open triangles), TAT (filled triangles), CTA (open pentagons), TAG (stars), versus the even values of the replication number r in DNA strands generated by the DNA polymerase Dpo1 from the archaeon *Sulfolobus solfataricus* P2 in a solution with the nucleotide concentrations (3). The initial DNA strand has the unequal mononucleotide fractions $A_0 = 70\%$, $C_0 = 15\%$, $G_0 = 10\%$, and $T_0 = 5\%$. The data points showing the results of the numerical simulation with Gillespie's algorithm are plotted every 200 replications. The solid lines depict the fractions predicted by theory. The asymptotic values of the fractions are given by $A = T = 43.8\%$, $C = G = 6.2\%$, $AT = TA = 19.2\%$, $AC = GT = 2.7\%$, $ATA = TAT = 8.4\%$, and $CTA = TAG = 1.2\%$, as obtained by averaging their values between the replications $r = 9900$ and $r = 10000$.

the concentrations.

Since the doubling time due to cell division is about 7-8 hr for *Sulfolobus solfataricus* [44, 45], the inverse η^{-1} of the polymerase error probability corresponds to a period of 1.2-1.7 yr for converging toward compliance, which is relatively short with respect to evolutionary time scales.

C. *Sulfolobus solfataricus* P2 DNA polymerase Dpo3

This other B-family polymerase of the same archaeon is also known to catalyze DNA replication, but at a slower rate and a lower fidelity than Dpo1. Its kinetic parameters, which have been measured experimentally for the lone polymerase activity [30], are reported in Table I.

Numerical simulations starting from an initial Bernoulli sequence with equal nucleotide fractions $A_0 = C_0 = G_0 = T_0 = 25\%$ show that the mononucleotide fractions converge toward asymptotic values over a shorter number of replications than Dpo1, because the error probability η is larger for Dpo3. Accordingly, the asymptotic values can here be calculated by averaging over the replications from $r = 900$ to $r = 1000$ and they are given in Table II. These asymptotic values depend on the nucleotide concentrations (2)-(4) considered in the simulations, but they comply with Chargaff's second parity rule.

D. *Sulfolobus solfataricus P2* DNA polymerase Dpo4

This further DNA polymerase from *Sulfolobus solfataricus P2* belongs to the family Y in charge of DNA repair. Its pre-steady-state kinetic parameters have been measured experimentally for the polymerase active site only [31] and they are presented in Table I. Its polymerization rate constants are larger than for Dpo3, but its fidelity is lower than for Dpo1.

For Dpo4, the asymptotic values of the mononucleotide fractions and the error probability are obtained by averaging over the replications between $r = 4500$ and $r = 5000$. They are given in Table II for the nucleotide concentrations (2)-(4). Again, Chargaff's second parity rule is very well satisfied.

E. *Thermococcus* species 9°N DNA polymerase

Thermococcus species 9°N is a thermophilic archaeon with a genome containing about 2×10^6 base pairs. The polymerase rate constants and dissociation constants have been measured experimentally for its exonuclease-deficient family-D DNA polymerase and their values are reported in Table I.

Numerical simulations of many successive replications again show that the mononucleotide fractions converge toward asymptotic values, which depend on the nucleotide concentrations, but comply with Chargaff's second parity rule. Table II gives these asymptotic values obtained by averaging over the replications between $r = 9900$ and $r = 10000$ for the concentrations (2)-(4).

For genus *Thermococcus*, cell division doubling times are observed in the range 24-95 min [46, 47]. In this case, the inverse η^{-1} of the polymerase error probability corresponds to a convergence period of 10-55 days, which is very short with respect to evolutionary time scales.

F. Rat DNA polymerase β

As a further example, we consider the wild-type (WT) rat DNA polymerase β . Rat is a mammal with a genome containing 2.9×10^9 base pairs in 22 chromosomes and characterized by the mononucleotide fractions $A \simeq T \simeq 29\%$ and $C \simeq G \simeq 21\%$. The polymerase β belongs to the X-family and acts in DNA repair pathways. This is an example of small eukaryotic polymerase without any exonuclease activity. The kinetic parameters of the WT rat DNA polymerase β have been experimentally measured using pre-steady-state kinetic methods and they are also reported in Table I [33].

For this polymerase, numerical simulations of many successive replications have also been carried out for the concentrations (2)-(4), starting from an initial Bernoulli sequence with $A_0 = C_0 = G_0 = T_0 = 25\%$. The convergence of the mononucleotide fractions toward asymptotic values compliant with Chargaff's second parity rule is again observed. These values are reported in Table II after averaging from $r = 9000$ to $r = 10000$.

G. Comparison between different polymerases and concentration values

The results of the numerical simulations show that the asymptotic values of the mononucleotide fractions depend on the type of polymerase carrying out the many successive replications and on the intracellular nucleotide concentrations. This observation suggests that the nucleotide fractions characterizing the genome of each species have evolved under the combined action of the different polymerases of the species, using intracellular nucleotide concentrations, which may vary in time during the cell cycle between two successive replications. In this regard, Table II shows that the physiological values (2) and (3) of the nucleotide concentrations tend to generate nucleotide fractions $A \simeq T$ that are larger than $C \simeq G$, as often observed in the genome of various organisms [8, 9, 12, 13, 26].

Nevertheless, the results of simulations show that Chargaff's second parity rule is always satisfied. At this stage, this numerical observation remains mysterious because the kinetic parameters reported in Table I take different values for the twelve incorrect base pairs. The purpose of the following Section III is to explain how Chargaff's second parity rule can hold in spite of such asymmetries.

III. THEORY FOR SUCCESSIVE DNA REPLICATIONS

A. Theory for a single DNA replication

During the last decade, important advances have been made in the theory of DNA replication and other template-directed copolymerization processes [27, 28, 41, 42, 48–58]. In particular, exact asymptotic solutions have been obtained for the replication of a template sequence $n_1 n_2 \cdots n_l \cdots n_L$ into a copy sequence $m_1 m_2 \cdots m_l \cdots m_L$ for different kinds of kinetics, depending or not on previously incorporated nucleotides, or on conformational changes of the polymerase [27, 28, 41, 42, 53]. In general, the attachment and detachment rates are specific to the polymerase and they depend on the nucleotide concentrations in the intracellular solution surrounding the polymerase. For Michaelis-Menten kinetics, the attachment and detachment rates have known mathematical expressions, which are given in Appendix A. For kinetics where the rates are independent of the previous incorporated nucleotide, theory shows that the copy forms a Bernoulli chain, so that the probability of finding some copy sequence grown on a given template sequence factorizes into the product of the probabilities of the individual nucleotides in the copy sequence [27, 41, 42].

Furthermore, for nucleotide concentrations such as (2)–(4) that are larger than their nanomolar chemical equilibrium values (where detailed balance holds and replication stops), the attachment rates are significantly larger than the detachment rates, so that the latter can be neglected in front of the former, $W_{+m_l, l} \gg W_{-m_l, l}$. These conditions are satisfied in the numerical simulations of Section II.

Under such circumstances, the conditional probability of finding the nucleotide m in the copy sequence and paired with the template nucleotide n can be expressed as

$$P_{\frac{m}{n}} \equiv \frac{W_{+m}}{\sum_{m'} W_{+m'}} \quad (5)$$

in terms of the attachment rates given by Eq. (A2). These conditional probabilities satisfy the following normalization conditions,

$$\sum_m P_{\frac{m}{n}} = 1 \quad \text{for all } n. \quad (6)$$

If the replication process starts with a template sequence forming a Bernoulli chain, the copy is again a Bernoulli chain, and this property persists upon further replications.

B. Extension to successive DNA replications

The conditional probabilities (5) allow us to determine the fractions or probabilities of nucleotides in all the copies generated by successive replications according to the process shown in Fig. 1. The nucleotide probabilities in the r^{th} sequence can be written in the form of the following column matrix or vector:

$$\mathbf{p}_r = \begin{bmatrix} A_r \\ C_r \\ G_r \\ T_r \end{bmatrix} \quad \text{such that} \quad A_r + C_r + G_r + T_r = 100\%. \quad (7)$$

Accordingly, the nucleotide probabilities of the sequence generated by the next replication are given by

$$\mathbf{p}_{r+1} = \mathbf{P} \cdot \mathbf{p}_r \quad (8)$$

in terms of the following 4×4 matrix containing the conditional probabilities (5):

$$\mathbf{P} \equiv \begin{bmatrix} P_{A A} & P_{A C} & P_{A G} & P_{A T} \\ P_{C A} & P_{C C} & P_{C G} & P_{C T} \\ P_{G A} & P_{G C} & P_{G G} & P_{G T} \\ P_{T A} & P_{T C} & P_{T G} & P_{T T} \end{bmatrix}, \quad (9)$$

which defines the matrix of transition probabilities, or more shortly transition matrix, for the process of interest [59, 60]. Probability is conserved, i.e., $A_{r+1} + C_{r+1} + G_{r+1} + T_{r+1} = 100\%$ also holds, because of the normalization conditions (6). The nucleotide probabilities of the r^{th} copy can thus be obtained by r successive matrix multiplications starting from the nucleotide probabilities of the initial template according to $\mathbf{p}_r = \mathbf{P}^r \cdot \mathbf{p}_0$. In particular, the error probability of the r^{th} replication is given by

$$\eta_r = 1 - P_{\text{A}} A_{r-1} - P_{\text{C}} C_{r-1} - P_{\text{G}} G_{r-1} - P_{\text{T}} T_{r-1} \quad (10)$$

in terms of the conditional probabilities (5) to form Watson-Crick complementary base pairs and the mononucleotide fractions \mathbf{p}_{r-1} in the template generating the copy in the replication. The error probability converges toward its asymptotic value $\eta = \lim_{r \rightarrow \infty} \eta_r$, which globally characterizes the replication errors made by the polymerase.

The theoretical predictions based on the matrix (9) are shown as solid lines in Figs. 2 and 3. They agree very well with the results of numerical simulations, confirming the validity of the theoretical assumptions. We note that the 4×4 matrix (9) is asymmetric, because polymerase kinetics are specific to the nucleotides involved in each reaction, which are of four different types, so that it is difficult in this regard to understand how the intrastrand symmetries observed in Figs. 2 and 3 can arise. Yet, the matrix (9) is not structureless.

The key point is that the (boxed) elements on the anti-diagonal of the matrix (9) are close to the value of 100%, because they give the probabilities of forming Watson-Crick complementary base pairs, while the other elements give the substitution probabilities for the formation of non-complementary base pairs. Accordingly, the matrix (9) can be decomposed as

$$\mathbf{P} = \mathbf{P}^{(0)} + \mathbf{P}^{(1)} \quad (11)$$

into its dominant part,

$$\mathbf{P}^{(0)} = \mathbf{C} \equiv \begin{bmatrix} 0 & 0 & 0 & 1 \\ 0 & 0 & 1 & 0 \\ 0 & 1 & 0 & 0 \\ 1 & 0 & 0 & 0 \end{bmatrix}, \quad (12)$$

and a rest given by another 4×4 matrix $\mathbf{P}^{(1)}$, which is of the order of the error probability η of the polymerase and which is thus significantly smaller than its dominant part (12). The latter is given by an anti-diagonal exchange matrix that directly expresses the Watson-Crick complementarity of the base pairs that are formed most often upon DNA replication. The rest $\mathbf{P}^{(1)}$ can be considered as a perturbation with respect to the dominant part and treated by perturbation theory using the error probability η and related quantities as small perturbation parameters.

C. Asymptotic behavior after many successive replications

The long-time behavior of the process can be expressed in terms of the four eigenvalues λ and the four associated eigenvectors \mathbf{v} of the transition matrix (5), such that $\mathbf{P} \cdot \mathbf{v} = \lambda \mathbf{v}$. The leading eigenvalue is equal to $\lambda = 1$, because the normalization conditions (6) are always satisfied. Therefore, we can obtain the asymptotic values of the nucleotide fractions or probabilities by calculating the leading eigenvector of the matrix (9), such that

$$\mathbf{v} = \mathbf{P} \cdot \mathbf{v}. \quad (13)$$

Now, the leading eigenvector can be expanded as the following series,

$$\mathbf{v} = \mathbf{v}^{(0)} + \mathbf{v}^{(1)} + \mathbf{v}^{(2)} + \dots \quad \text{with} \quad \mathbf{v}^{(n)} = O(\eta^n), \quad (14)$$

going as powers of the small parameter. Inserting the decomposition (11) and the expansion (14) into Eq. (13) and identifying the terms corresponding to the same power of the small parameter, we obtain the following equations at the different orders of perturbation:

$$\text{order 0: } (\mathbf{1} - \mathbf{C}) \cdot \mathbf{v}^{(0)} = 0, \quad (15)$$

$$\text{order 1: } (\mathbf{1} - \mathbf{C}) \cdot \mathbf{v}^{(1)} = \mathbf{P}^{(1)} \cdot \mathbf{v}^{(0)}, \quad (16)$$

⋮

Given the form (12) of the anti-diagonal exchange matrix \mathbf{C} , Eq. (15) at order 0 gives the following solutions:

$$\mathbf{v}^{(0)} = \begin{bmatrix} A^{(0)} \\ C^{(0)} \\ G^{(0)} \\ T^{(0)} \end{bmatrix} \quad \text{with} \quad A^{(0)} = T^{(0)} \quad \text{and} \quad C^{(0)} = G^{(0)}. \quad (17)$$

Therefore, at order 0, we obtain the exact equality between the fractions of complementary base pairs, underlying Chargaff's second parity rule. However, since this solution is degenerate, we still need to consider Eq. (16) at order 1, which explicitly reads

$$\begin{bmatrix} A^{(1)} - T^{(1)} \\ C^{(1)} - G^{(1)} \\ -C^{(1)} + G^{(1)} \\ -A^{(1)} + T^{(1)} \end{bmatrix} = \mathbf{P}^{(1)} \cdot \begin{bmatrix} A^{(0)} \\ C^{(0)} \\ C^{(0)} \\ A^{(0)} \end{bmatrix}, \quad (18)$$

because of Eqs. (12) and (17).

Multiplying this equation from its left-hand side by the row matrices $[1\ 0\ 0\ 1]$ and $[0\ 1\ 1\ 0]$, we obtain the following expressions for the asymptotic nucleotide fractions at order 0:

$$A^{(0)} = T^{(0)} = \frac{P_C + P_G + P_T + P_G}{2(P_C + P_G + P_T + P_G + P_C + P_G + P_T + P_G)}, \quad (19)$$

$$C^{(0)} = G^{(0)} = \frac{P_A + P_G + P_C + P_T}{2(P_C + P_G + P_T + P_G + P_C + P_G + P_T + P_G)}. \quad (20)$$

Next, if we multiply Eq. (18) from its left-hand side by the row matrices $[1\ 0\ 0\ 0]$ and $[0\ 1\ 0\ 0]$, we obtain the corrections to the nucleotide fractions at next order: $A^{(1)} - T^{(1)} = O(\eta) \neq 0$ and $C^{(1)} - G^{(1)} = O(\eta) \neq 0$. These corrections do not satisfy the strict equalities between the fractions of the complementary base pairs, but the differences are of the order of the error probability η of the polymerase, which is typically very small. The intrastrand symmetry is thus only approximate in agreement with observations. Therefore, this reasoning explains Chargaff's second parity rule stated as the *approximate* equality between the intrastrand fractions of complementary nucleotides, since the equality only holds with an accuracy of the order of the polymerase error probability.

We note that, in the particular case where the replication process was homogeneous with conditional probabilities that are all equal to $P_n^m = 1 - \eta$ for complementary pairs $m = \tilde{n}$ and to $P_n^m = \eta/3$ for non-complementary pairs $m \neq \tilde{n}$, the asymptotic nucleotide fractions would all be equal to each other with $A = C = G = T = 25\%$.

Since the successive copies form Bernoulli chains, the fractions of the oligonucleotides are here given by products of mononucleotide fractions as $p(m_1 m_2 \cdots m_l) = \prod_{j=1}^l p(m_j)$. This prediction is indeed confirmed by the results of the numerical simulations shown in Figs. 2 and 3.

D. Transient behavior before convergence

The transient behavior of the replication process can be characterized in terms of the whole set of four eigenvalues and eigenvectors of the matrix (9). The leading eigenvalue is always equal to one, but the next-to-leading eigenvalues are not and they can be expanded in powers of the error probability η as $\lambda = \lambda^{(0)} + \lambda^{(1)} + \lambda^{(2)} + \cdots$ with $\lambda^{(n)} = O(\eta^n)$. At order 0, the four eigenvalues $\lambda^{(0)}$ are given by $\{+1, +1, -1, -1\}$. At order 1, the corrections $\lambda^{(1)}$ are evaluated as $\{0, O(\eta), O(\eta), O(\eta)\}$, respectively. Typically, the three non-leading eigenvalues have an absolute value lower than one, $|\lambda| < 1$, expressing the fact that the nucleotide fractions converge toward the values fixed by the leading eigenvector associated with the eigenvalue $\lambda = 1$. There are thus three modes of relaxation toward the asymptotic values: a mode of exponential relaxation corresponding to $0 < \lambda < 1$ and two other modes corresponding to $0 < |\lambda| < 1$ with $\lambda^{(0)} = -1$. For each mode, the time scale of relaxation is given by $\tau = (-\ln |\lambda|)^{-1}$, which is measured in replication number.

E. Example

As an example, we consider the multireplication process for the DNA polymerase Dpo1 from the archeon *Sulfolobus solfataricus P2* at the physiological concentrations (3). In this case, the matrix (9) can be formed with the elements (5)

using the polymerization rate and dissociation constants given in Table I and its eigenvalues λ can be computed to be $\{1, 0.998292, -0.999092, -0.998519\}$. The eigenvector associated with the leading eigenvalue $\lambda = 1$ and its approximation at order 0, which is given by Eqs. (19) and (20), have the following evaluations, respectively:

$$\mathbf{v} = \begin{bmatrix} 43.7985\% \\ 6.1930\% \\ 6.2039\% \\ 43.8046\% \end{bmatrix} \quad \text{and} \quad \mathbf{v}^{(0)} = \begin{bmatrix} 43.8001\% \\ 6.1999\% \\ 6.1999\% \\ 43.8001\% \end{bmatrix}, \quad (21)$$

confirming that the equality between the fractions of complementary bases is only approximate, although the differences are of the order of the polymerase error probability $\eta = 0.00066$, which is very small, and, thus, undetectable with the accuracy used in Table II for presenting the results of numerical simulations with this polymerase. Nevertheless, we note that small deviations with respect to the strict equality are visible for the cases where the error probability is the largest in Table II, which supports the statement that approximate equality between complementary-base fractions is controlled by the smallness of the polymerase error probability.

Moreover, going back to the polymerase Dpo1 at concentrations (3), the relaxation time scales of the replication process can be evaluated by $(-\ln |\lambda|)^{-1}$ in terms of the four eigenvalues λ and they are given by $\{\infty, 584.8, 1100.8, 674.9\}$, respectively. These values are the numbers of replications, over which the amplitude of the relaxation mode is reduced by a factor $e \simeq 2.718$. For a process starting from equal nucleotide fractions, the approximate equalities $A_r \simeq T_r$ and $C_r \simeq G_r$ are maintained since the beginning of the process, as seen in Fig. 2. In this case, the relaxation toward the asymptotic values (21) is essentially controlled by the eigenvalue $\lambda = 0.998292$ corresponding to a relaxation over the time scale $(-\ln |\lambda|)^{-1} = 584.8$, which is observed in Fig. 2. However, if the process starts from unequal nucleotide fractions, the relaxation involves all the eigenvalues and, in particular, the eigenvalues with a negative real part, which generate nucleotide fractions that alternate between odd and even replication numbers. This alternating behavior is not seen in Fig. 3 because the fractions are plotted therein only at even replication numbers. The fractions at odd replication numbers are actually close to the plotted fractions of the complementary base. The relaxation mode associated with the eigenvalue $\lambda = -0.999092$ is slower since its relaxation time scale is given by $(-\ln |\lambda|)^{-1} = 1100.8$, which is indeed what is observed in Fig. 3. The other eigenvalue $\lambda = -0.998519$ has a similar effect, but over the intermediate time scale $(-\ln |\lambda|)^{-1} = 674.9$.

Therefore, the theory can explain the multireplication process in great detail.

IV. KINETICS WITH A DEPENDENCE ON THE PREVIOUSLY INCORPORATED NUCLEOTIDE

In general, the kinetics of polymerases depend not only on the ultimate pair $m_l : n_l$ of nucleotides, which is formed during the elongation of the copy, but also on the previously incorporated nucleotide m_{l-1} and, thus, on the penultimate pair $m_{l-1} : n_{l-1}$ [27, 28, 41, 42]. Such dependences have been measured experimentally. In particular, polymerases are known to slow down if the previously incorporated nucleotide is incorrect [40]. Therefore, it is important to extend the study to such more complicated kinetics to evaluate the consequences of the dependence on further nucleotides.

A. Numerical simulations

As before, the replication process (1) can be numerically simulated using Gillespie's algorithm [34, 35], now with an extended dependence of the attachment and detachment rates $W_{\pm m_l, l}$ on the penultimate pair $m_{l-1} : n_{l-1}$. Assuming that the polymerase has Michaelis-Menten kinetics, the rates are given by expressions similar to Eqs. (A2) and (A3), after replacing the polymerization rate constants with $k_{+m_l|n_l|n_{l-1}}^P$ and the dissociation constants with $K_{+m_l|n_l|n_{l-1}}^{+m_l|n_{l-1}}$ [28, 41]. Nevertheless, experimental data are sparse and these constants are often only known if the pairs are either correct (c) or incorrect (i) [40].

Here, we focus on the exonuclease-deficient DNA polymerase Dpo1 from the archaeon *Sulfolobus solfataricus* P2, taking the values of Table I for the polymerization rate constants $k_{+m_l|n_l|c}^P = k_{+m_l|n_l}^P$ and the dissociation constants $K_{+m_l|n_l|c} = K_{+m_l|n_l}^P$ after correct incorporation; and the polymerization rate constants after incorrect incorporation as

$$k_{+c|i}^P = 0.13 \text{ s}^{-1}, \quad k_{+i|i}^P = 0.001 \text{ s}^{-1}, \quad (22)$$

and the corresponding dissociation constants as

$$K_{c|i} = 1000 \mu\text{M}, \quad K_{i|i} = 2600 \mu\text{M}, \quad (23)$$

for $\frac{m_l}{n_l} |_{n_{l-1}}^{m_{l-1}} = c|i$ or $i|i$, respectively [29].

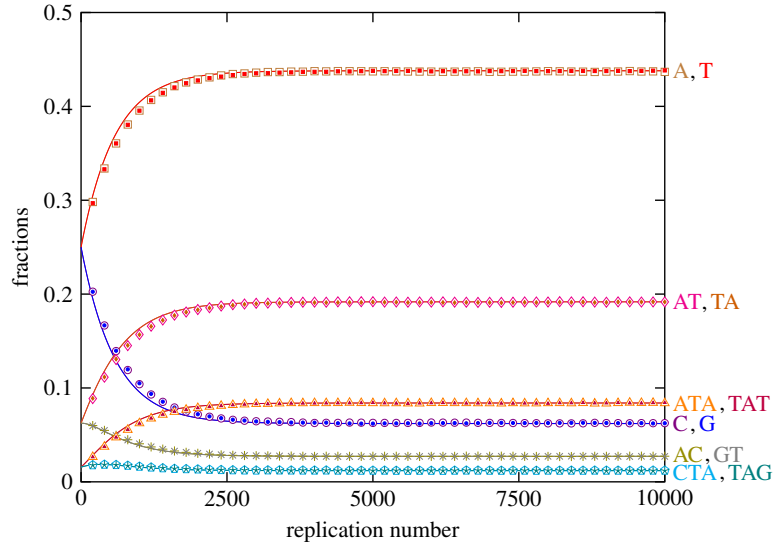


FIG. 4: Fractions of the mononucleotides A (open squares), T (filled squares), C (open circles), G (filled circles), binucleotides AT (open diamonds), TA (filled diamonds), AC (pluses), GT (times), and trinucleotides ATA (open triangles), TAT (filled triangles), CTA (open pentagons), TAG (stars), versus the even values of the replication number r in DNA strands generated by the DNA polymerase Dpo1 from the archaeon *Sulfolobus solfataricus* P2 in a solution with the nucleotide concentrations (3), here, for the kinetics depending on the previously incorporated nucleotide with the constants (22) and (23). The initial DNA strand has equal mononucleotide fractions $A_0 = C_0 = G_0 = T_0 = 25\%$. The data points showing the results of the numerical simulation with Gillespie's algorithm are plotted every 200 replications. The solid lines depict the fractions predicted by theory. The asymptotic values of the fractions are given by $A = T = 43.8\%$, $C = G = 6.2\%$, $AT = TA = 19.2\%$, $AC = GT = 2.7\%$, $ATA = TAT = 8.4\%$, and $CTA = TAG = 1.2\%$, as obtained by averaging their values between the replications $r = 9900$ and $r = 10000$.

The results of the numerical simulations are shown in Fig. 4 starting from an initial template with equal nucleotide fractions (as in Fig. 2); and in Fig. 5 starting from initial unequal fractions (as in Fig. 3); in both cases with the nucleotide concentrations (3). Again, after many successive replications, we observe the convergence of the mono- and oligonucleotide fractions toward asymptotic values complying with Chargaff's second parity rule. Numerical simulations have also been performed for the two other sets of concentrations (2) and (4) and the asymptotic mononucleotide fractions of these simulations are presented in Table III.

TABLE III: Asymptotic values of the nucleotide fractions and the corresponding error probability η for the numerical simulations with Gillespie's algorithm of many successive DNA replications with the exonuclease-deficient DNA polymerase from *Sulfolobus solfataricus* P2, here, for the kinetics depending on the previously incorporated nucleotide with the constants (22) and (23). In every case, the initial template sequence has equal fractions of nucleotides. The concentrations I-III are given by Eqs. (2)-(4). The statistical errors are smaller than the last digit shown.

DNA polymerase	concentrations	$A(\%)$	$T(\%)$	$C(\%)$	$G(\%)$	η
<i>Sulf. solf. Dpo1</i>	I	45.3	45.3	4.7	4.7	0.00027
	II	43.8	43.8	6.2	6.2	0.00057
	III	33.0	33.0	17.0	17.0	0.00066

In Figs. 4 and 5, we also observe that the inclusion of a dependence on the previously incorporated nucleotide does not significantly change the results. The asymptotic values of the nucleotide fractions are modified, but by

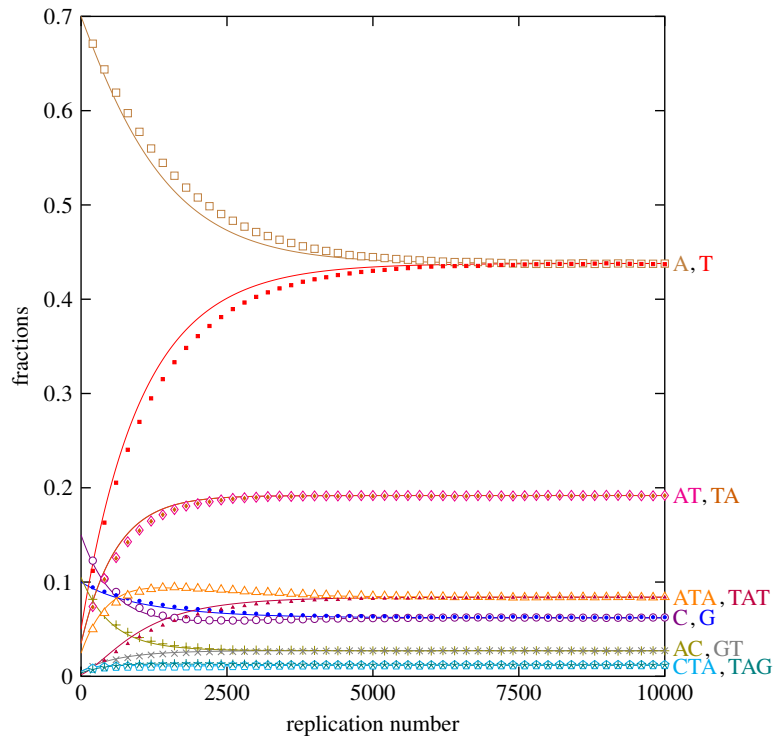


FIG. 5: Fractions of the mononucleotides A (open squares), T (filled squares), C (open circles), G (filled circles), binucleotides AT (open diamonds), TA (filled diamonds), AC (pluses), GT (times), and trinucleotides ATA (open triangles), TAT (filled triangles), CTA (open pentagons), TAG (stars), versus the even values of the replication number r in DNA strands generated by the DNA polymerase Dpo1 from the archaeon *Sulfolobus solfataricus* *P2* in a solution with the nucleotide concentrations (3), here, for the kinetics depending on the previously incorporated nucleotide with the constants (22) and (23). The initial DNA strand has the unequal mononucleotide fractions $A_0 = 70\%$, $C_0 = 15\%$, $G_0 = 10\%$, and $T_0 = 5\%$. The data points showing the results of the numerical simulation with Gillespie's algorithm are plotted every 200 replications. The solid lines depict the fractions predicted by theory. The asymptotic values of the fractions are given by $A = T = 43.8\%$, $C = G = 6.2\%$, $AT = TA = 19.2\%$, $AC = GT = 2.7\%$, $ATA = TAT = 8.4\%$, and $CTA = TAG = 1.2\%$, as obtained by averaging their values between the replications $r = 9900$ and $r = 10000$.

small amounts, as seen by comparing the values given in Tables II and III for the polymerase Dpo1 from *Sulfolobus solfataricus* *P2*. The results generated by the kinetics with a dependence on the previously incorporated nucleotide turn out to be close to those of Section II, which have been obtained without this dependence.

B. Theory

Theory shows that, in general, kinetics depending on penultimate pairs generate sequences forming Markov chains [27, 28, 41, 42]. As aforementioned, for the concentration sets (2)-(4), the detachment rates are negligible in front of the attachment rates, $W_{+m_l,l} \gg W_{-m_l,l}$.

Under such circumstances, the conditional probability to form the ultimate pair $m:n$ provided that the penultimate pair (x) is either correct (c) or incorrect (i) is given by

$$P_{\frac{m}{n}|x} \equiv \frac{W_{\frac{+m}{n}|x}}{\sum_{m'} W_{\frac{+m'}{n}|x}} \quad \text{for} \quad x = c, i \quad (24)$$

in terms of the corresponding attachment rates $W_{\frac{+m}{n}|x}$ [28, 41].

After many successive replications, the error probability of the replication process reaches the asymptotic value η given in Table III. Therefore, along a template sequence, the fraction of correct penultimate pairs is equal to $(1 - \eta)$ and the fraction of incorrect ones to η . Thus, a possible approximation consists in supposing that the matrix of

conditional probabilities can be taken as an average over correct and incorrect penultimate pairs as

$$\mathbf{P} = (1 - \eta) \mathbf{P}_c + \eta \mathbf{P}_i \quad \text{with} \quad \mathbf{P}_x = \left[P_{\frac{m}{n}|x} \right] \quad \text{for } x = c, i. \quad (25)$$

Therefore, the nucleotide fractions or probabilities after r replications can be evaluated by matrix multiplication according to $\mathbf{p}_r = \mathbf{P}^r \cdot \mathbf{p}_0$, where \mathbf{p}_0 is the vector of initial fractions. In this approximation, the memory of the previously incorporated nucleotide is neglected and the effective replication process reduces to one generating Bernoulli chains (rather than Markov chains).

In Figs. 4 and 5, the solid lines show the results of these theoretical predictions. We observe agreement between the approximations based on the matrix (25) and the results of the numerical simulation of the complete process with Gillespie's algorithm. The agreement is excellent for the asymptotic values of the mono- and oligonucleotide fractions. This observation shows that the sequences generated by the replication process are close to be Bernoulli chains and that they have a negligible Markovian character. Nevertheless, deviations between theory and numerical simulations are observed in the transient behavior. A possible reason for these deviations is that the error probability η_r depends in general on the sequence that is copied and, thus, on the replication number r . Therefore, the approximation (25), which consists in replacing the current error probability by its asymptotic value $\eta = \lim_{r \rightarrow \infty} \eta_r$, can only be valid in the asymptotic regime and should not be expected to apply during transients.

C. DNA polymerases with exonuclease proofreading

In addition to the domain of their genuine polymerase activity, most DNA polymerases have another domain with an exonuclease activity, which has a proofreading effect on replication [1]. This error-correction mechanism uses the dependence of the polymerase activity on the previously incorporated nucleotide [40]. If polymerization is slowed down by the insertion of an incorrect nucleotide, the DNA chain has the time to jump to the exonuclease domain, where the incorrect nucleotide is cleaved by hydrolysis, lowering the error probability η by a factor of about 10^2 . Kinetic theory shows that the rates of exonuclease activity are added to the rates of the polymerase activity [52]. Since the error probability is lower, complementarity is stronger between the copy and the template upon replication, reinforcing the dominant role of the anti-diagonal exchange matrix (12) at the basis of Chargaff's second parity rule. However, the convergence toward compliance would be delayed by the factor enhancing the fidelity of such DNA polymerases with exonuclease proofreading.

V. CONCLUSION AND PERSPECTIVES

In this paper, the DNA multireplication process schematically represented in Fig. 1 was numerically simulated for five different DNA polymerases in order to test the validity of Chargaff's second parity rule. Every replication proceeds by the template-directed elongation of the copy, binding one by one the monomeric units, i.e., the nucleotides forming base pairs with the template according to the biochemical kinetics of the DNA polymerase. Many replications are successively performed to simulate the molecular evolution of the DNA sequence under the effect of the point-like mutations due to nucleotide substitutions by the polymerase according to its error probability η . After a number of replications of the order of the inverse η^{-1} of the polymerase error probability, the fractions of mono- and oligonucleotides are observed to converge toward compliance with Chargaff's second parity rule, i.e., toward approximate equalities between the intrastrand fractions of complementary mono- and oligonucleotides. These numerical observations are confirmed with the theory of the multireplication process of Fig. 1.

For polymerase kinetics independent of the previously incorporated nucleotide, the copy forms a Bernoulli chain and the replication process is ruled by a four-by-four transition matrix, giving the evolution of the intrastrand nucleotide fractions during the process. This transition matrix has a most remarkable structure:

- (1) its dominant part is a four-by-four anti-diagonal exchange matrix, expressing the fact that DNA replication would copy a nucleotide into the complementary nucleotide if there was no replication error;
- (2) the rest of the transition matrix is of the order of the polymerase error probability η .

The multireplication process evolves by many iterations generated by matrix multiplication. Under this process, the intrastrand nucleotide fractions converge toward stationary values (A, C, G, T) given by the eigenvector of the transition matrix that is associated with the leading eigenvalue equal to the unit value, $\lambda = 1$. These asymptotic intrastrand nucleotide fractions satisfy the equalities $A^{(0)} = T^{(0)}$ and $C^{(0)} = G^{(0)}$ at order 0 of a series expansion in powers of the polymerase error probability η . The equalities are no longer satisfied at higher orders $O(\eta^n)$: $A^{(n)} \neq T^{(n)}$

and $C^{(n)} \neq G^{(n)}$ for $n \geq 1$. Therefore, theory demonstrates that the equalities between the asymptotic intrastrand fractions of complementary nucleotides are approximate with possible deviations of the order of the polymerase error probability, $|A - T| = O(\eta)$ and $|C - G| = O(\eta)$, which is in accordance with Chargaff's second parity rule. The higher the fidelity η^{-1} of the polymerase, the closer the equalities between the fractions of complementary nucleotides. The fractions of oligonucleotides behave similarly.

Theory also shows that the relaxation toward compliance with Chargaff's second parity rule is determined by the three eigenvalues beyond the leading one ($\lambda = 1$), which have typically an absolute value smaller than the unit value by a quantity of the order of the error probability: $|\lambda| < 1$ and $1 - |\lambda| = O(\eta)$. Accordingly, the time scale of relaxation toward compliance (measured in number of replications) is of the order of the inverse of the polymerase error probability η^{-1} . As a consequence, the higher the fidelity of the polymerase, the longer the relaxation toward compliance with Chargaff's second parity rule. The relaxation time scale can be evaluated as the inverse error probability multiplied by the doubling time of organisms, which gives relatively short periods of time with respect to evolutionary time scales for unicellular organisms.

The results extend to more complicated polymerase kinetics having a dependence on the previously incorporated nucleotide.

Furthermore, the study shows that the asymptotic nucleotide fractions depend on the kinetics of the polymerase and on the intracellular concentrations of the four nucleotides. The latter are regulated by the nucleotide metabolism of the cell. Interestingly, for typical polymerases and known physiological values of the nucleotide concentrations, the DNA nucleotide content is found to be more abundant in adenine and thymine than in cytosine and guanine, i.e., $A + T > C + G$, which corresponds to what is observed for the DNA of many species [8, 9, 12, 13, 26].

The mechanism, which is here theoretically studied, could be tested by automated experiments of multiple DNA replications successively performed by some DNA polymerase starting from some initial DNA sequence.

We emphasize that the model, which is used as the vehicle of this study, is far from realistic. In general, replication is carried out by several types of polymerases and the intracellular nucleotide concentrations may vary during the different phases of cell division. Accordingly, the expectation is that the DNA nucleotide fractions should result from an average over the different steps of replication. Nevertheless, all the polymerases replicate every DNA strand into a mostly complementary strand, so that the main features of replication are essentially captured by the model of Fig. 1. In this regard, the replication process based on the biochemical kinetics of polymerases provides a robust mechanism underlying the approximate intrastrand symmetry expressed by Chargaff's second parity rule. The polymerase kinetics generate point-like mutations caused by nucleotide substitutions, which drives the molecular evolution of DNA sequences toward compliance with Chargaff's second parity rule. There is an evolutionary advantage for the genome to remain close to compliance. Otherwise, the genome would drift away from its selected composition because of mutational pressure.

Finally, we remark that the robustness of the mechanism based on the kinetics of DNA polymerases suggests that the strong deviations with respect to Chargaff's second parity rule, which are observed in the genome of mammalian mitochondria and in some single-stranded DNA viruses [14, 15], might be caused by the interference of DNA replication with other processes such as transcription [61] in combination with the smallness of these genomes. Future studies should address this open issue.

Acknowledgments

This research is supported by the Université libre de Bruxelles (ULB).

Appendix A: Mathematical formulation of replication kinetics

1. Kinetic equations

The replication process (1) is ruled by the following kinetic equations [51],

$$\begin{aligned} \frac{d}{dt} P_t \left(\begin{matrix} m_1 \cdots m_l \\ n_1 \cdots n_l n_{l+1} \cdots \end{matrix} \right) &= W_{+m_l, l} P_t \left(\begin{matrix} m_1 \cdots m_{l-1} \\ n_1 \cdots n_{l-1} n_l \cdots \end{matrix} \right) \\ &+ \sum_{m_{l+1}} W_{-m_{l+1}, l+1} P_t \left(\begin{matrix} m_1 \cdots m_l m_{l+1} \\ n_1 \cdots n_l n_{l+1} n_{l+2} \cdots \end{matrix} \right) \\ &- \left(W_{-m_l, l} + \sum_{m_{l+1}} W_{+m_{l+1}, l+1} \right) P_t \left(\begin{matrix} m_1 \cdots m_l \\ n_1 \cdots n_l n_{l+1} \cdots \end{matrix} \right), \end{aligned} \quad (\text{A1})$$

for the probabilities of all the copy sequences $m_1, m_1 m_2, \dots, m_1 \cdots m_l, \dots$, which may be generated along the template sequence $n_1 \cdots n_l n_{l+1} \cdots$. In these kinetic equations, $W_{\pm m_l, l}$ respectively denote the attachment and detachment rates of the nucleotide m_l at the location l of the template. The polymerases are enzymes, which basically obey Michaelis-Menten kinetics [36, 38, 39]. The mathematical expressions of the rates are known whether the kinetics of the polymerase depend or not on the previously incorporated nucleotide [27, 28, 41, 51].

2. Kinetics independent of previously incorporated nucleotide

For kinetics independent of the previously incorporated nucleotide (as considered in Sections II and III), the attachment and detachment rates can be expressed in terms of the constants $k_{\pm m_l}^P$ for the polymerization and depolymerization of m_l after its pairing with n_l and the dissociation constant $K_{n_l}^{m_l}$ of the pair $m_l : n_l$. Moreover, these rates depend on the concentrations $[m_l \text{PP}]$ of the deoxyribonucleoside triphosphates $m_l \text{PP}$ and on the concentration $[\text{PP}]$ of pyrophosphate PP . The concentration unit is the *mole per liter* (M). With these notations, the attachment rate of m_l is given by

$$W_{+m_l, l} = W_{\frac{n_l}{m_l}} = \frac{k_{+m_l}^P [m_l \text{PP}]}{K_{n_l}^{m_l} Q_{n_l}} \quad (\text{A2})$$

and the detachment rate of m_l by

$$W_{-m_l, l} = W_{\frac{-m_l}{n_{l+1} n_l}} = \frac{k_{-m_l}^P [\text{PP}]}{Q_{n_{l+1}}}, \quad (\text{A3})$$

where

$$Q_{n_l} \equiv 1 + \sum_{m_l} \frac{[m_l \text{PP}]}{K_{n_l}^{m_l}} \quad (\text{A4})$$

is the Michaelis-Menten denominator [51]. We note that the denominator in the depolymerization rate (A3) is shifted by one unit with respect to the denominator in the polymerization rate (A2) because the rapid intermediate step of the Michaelis-Menten kinetics is the formation of the pair $m_l : n_l$ for the forward reaction, but that of the pair $m_{l+1} : n_{l+1}$ for the backward reaction [51].

Experimental data being rare for the depolymerization rate constants, it is assumed for simplicity that they are proportional to the corresponding polymerization rate constant according to

$$k_{-m_l}^P = \frac{1}{K_P} k_{+m_l}^P, \quad (\text{A5})$$

where the constant associated with pyrophosphorolysis is here supposed to take the value $K_P = 200 \text{ mM}$ [51]. The physiological concentration of pyrophosphate is typically given by $[\text{PP}] = 10^{-4} \text{ M}$ [62].

3. Kinetics with a dependence on previously incorporated nucleotide

For such kinetics, the constants also depend on the penultimate pair $m_{l-1} : n_{l-1}$ [27, 28, 41, 42]. Accordingly, the attachment and detachment rates are given by similar expressions as Eqs. (A2)-(A4), but with the constants $k_{\pm m_l}^p$ and $K_{n_l}^{m_l}$ replaced with $k_{\pm m_l}^p|_{n_l}^{m_{l-1}}$ and $K_{n_l}^{m_l}|_{n_l}^{m_{l-1}}$, respectively.

[1] B. Alberts, D. Bray, J. Lewis, M. Raff, K. Roberts, and J. D. Watson, *Molecular Biology of the Cell*, 2nd Edition (Garland Publishing, New York & London, 1989).

[2] E. Chargaff, *Chemical Specificity of Nucleic Acids and Mechanism of their Enzymatic Degradation*, *Experientia* **6**, 201–209 (1950).

[3] E. Chargaff, *Structure and function of nucleic acids as cell constituents*, *Fed. Proc.* **10**, 654–659 (1951).

[4] E. Chargaff, R. Lipshitz, C. Green, and M. E. Hodes, *The composition of the desoxyribonucleic acid of salmon sperm*, *J. Biol. Chem.* **191**, 223–230 (1951).

[5] E. Chargaff, R. Lipshitz, and C. Green, *Composition of the desoxypentose nucleic acids of four genera of sea-urchin*, *J. Biol. Chem.* **195**, 155–160 (1952).

[6] J. D. Watson and F. H. C. Crick, *Molecular structure of nucleic acids*, *Nature* **171**, 737–738 (1953).

[7] J. D. Watson and F. H. C. Crick, *Genetical implications of the structure of deoxyribonucleic acid*, *Nature* **171**, 964–967 (1953).

[8] J. D. Karkas, R. Rudner, and E. Chargaff, *Separation of *B. subtilis* DNA into complementary strands. II. Template functions and composition as determined by transcription with RNA polymerase*, *Proc. Natl. Acad. Sci. USA* **60**, 915–920 (1968).

[9] R. Rudner, J. D. Karkas, and E. Chargaff, *Separation of *B. subtilis* DNA into complementary strands. III. Direct analysis*, *Proc. Natl. Acad. Sci. USA* **60**, 921–922 (1968).

[10] V. V. Prabhu, *Symmetry observations in long nucleotide sequences*, *Nucl. Acids Res.* **21**, 2797–2800 (1993).

[11] D. Qi and A. J. Cuticchia, *Compositional symmetries in complete genomes*, *Bioinformatics* **17**, 557–559 (2001).

[12] P.-F. Baisnée, S. Hampson, and P. Baldi, *Why are complementary DNA strands symmetric?*, *Bioinformatics* **18**, 1021–1033 (2002).

[13] A. Provata, C. Nicolis, and G. Nicolis, *Complexity measures for the evolutionary categorization of organisms*, *Comput. Biol. Chem.* **53**, 5–14 (2014).

[14] D. Mitchell and R. Bridge, *A test of Chargaff's second rule*, *Biochem. Biophys. Res. Commun.* **340**, 90–94 (2006).

[15] C. Nikolaou and Y. Almirantis, *Deviations from Chargaff's second parity rule in organellar DNA Insights into the evolution of organellar genomes*, *Gene* **381**, 34–41 (2006).

[16] N. Sueoka, *Intrastrand Parity Rules of DNA Base Composition and Usage Biases of Synonymous Codons*, *J. Mol. Evol.* **40**, 318–325 (1995); *Erratum*, *J. Mol. Evol.* **42**, 323 (1996).

[17] J. R. Lobry, *Properties of a General Model of DNA Evolution Under No-Strand-Bias Conditions*, *J. Mol. Evol.* **40**, 326–330 (1995); *Erratum*, *J. Mol. Evol.* **41**, 680 (1995).

[18] A. Hart, S. Martínez, and F. Olmos, *A Gibbs Approach to Chargaff's Second Parity Rule*, *J. Stat. Phys.* **146**, 408–422 (2012).

[19] P. Fariselli, C. Taccioli, L. Pagani, and A. Maritan, *DNA sequence symmetries from randomness: the origin of the Chargaff's second parity rule*, *Briefings in Bioinform.* **22**, 2172–2181 (2021).

[20] P. Pflughaupt and A. B. Sahakyan, *Generalised interrelations among mutation rates drive the genomic compliance of Chargaff's second parity rule*, *Nucl. Acids Res.* **51**, 7409–7423 (2023).

[21] D. R. Forsdyke, *Relative Roles of Primary Sequence and (G + C)% in Determining the Hierarchy of Frequencies of Complementary Trinucleotide Pairs in DNAs of Different Species*, *J. Mol. Evol.* **41**, 573–581 (1995).

[22] S. J. Bell and D. R. Forsdyke, *Accounting Units in DNA*, *J. Theor. Biol.* **197**, 51–61 (1999).

[23] S. J. Bell and D. R. Forsdyke, *Deviations from Chargaff's Second Parity Rule Correlate with Direction of Transcription*, *J. Theor. Biol.* **197**, 63–76 (1999).

[24] G. Albrecht-Buehler, *Asymptotically increasing compliance of genomes with Chargaff's second parity rules through inversions and inverted transpositions*, *Proc. Natl. Acad. Sci. USA* **103**, 17828–17833 (2006).

[25] G. Albrecht-Buehler, *Inversions and inverted transpositions as the basis for an almost universal "format" of genome sequences*, *Genomics* **90**, 297–305 (2007).

[26] K. Okamura, J. Wei, and S. W. Scherer, *Evolutionary implications of inversions that have caused intra-strand parity in DNA*, *BMC Genomics* **8**, 160 (2007).

[27] P. Gaspard, *Kinetics and thermodynamics of living copolymerization processes*, *Phil Trans. R. Soc. A* **374**, 20160147 (2016); *Erratum*, *ibid.* **375**, 20170053 (2017).

[28] P. Gaspard, *Iterated function systems for DNA replication*, *Phys. Rev. E* **96**, 042403 (2017).

[29] L. Zhang, J. A. Brown, S. A. Newmister, and Z. Suo, *Polymerization Fidelity of a Replicative DNA Polymerase from the Hyperthermophilic Archaeon *Sulfolobus solfataricus* P2*, *Biochem.* **48**, 7492–7501 (2009).

[30] R. J. Bauer, M. T. Begley, and M. A. Trakselis, *Kinetics and Fidelity of Polymerization by DNA Polymerase III from*

Sulfolobus solfataricus, Biochem. **51**, 1996–2007 (2012).

[31] K. A. Fiala and Z. Suo, *Pre-Steady-State Kinetic Studies of the Fidelity of Sulfolobus solfataricus P2 DNA Polymerase IV*, Biochem. **43**, 2106–2115 (2004).

[32] K. M. Schermerhorn and A. F. Gardner, *Pre-steady-state Kinetic Analysis of a Family D DNA Polymerase from Thermo-coccus sp. 9°N Reveals Mechanisms for Archaeal Genomic Replication and Maintenance*, J. Biol. Chem. **290**, 21800–21810 (2015).

[33] J. Ahn, B. G. Werneburg, and M.-D. Tsai, *DNA Polymerase β : Structure–Fidelity Relationship from Pre-Steady-State Kinetic Analyses of All Possible Correct and Incorrect Base Pairs for Wild Type and R283A Mutant*, Biochem. **36**, 1100–1107 (1997).

[34] D. T. Gillespie, *A general method for numerically simulating the stochastic time evolution of coupled chemical reactions*, J. Comput. Phys. **22**, 403–434 (1976).

[35] D. T. Gillespie, *Exact stochastic simulation of coupled chemical reactions*, J. Phys. Chem. **81**, 2340–2361 (1977).

[36] L. Michaelis and M. L. Menten, *Die Kinetik der Invertinwirkung*, Biochem. Z. **49**, 333–369 (1913); English translation in Ref. [37].

[37] K. A. Johnson and R. S. Goody, *The Original Michaelis Constant: Translation of the 1913 Michaelis–Menten Paper*, Biochem. **50**, 8264–8269 (2011).

[38] L. Stryer, *Biochemistry*, 2nd Edition (Freeman and Co., San Francisco, 1981).

[39] A. L. Lehninger, *Principles of Biochemistry* (Worth Publishers, New York, 1982).

[40] K. A. Johnson, *Conformational Coupling in DNA Polymerase Fidelity*, Annu. Rev. Biochem. **62**, 685–713 (1993).

[41] P. Gaspard, *Template-Directed Copolymerization, Random Walks along Disordered Tracks, and Fractals*, Phys. Rev. Lett. **117**, 238101 (2016).

[42] P. Gaspard, *Kinetic theory and thermodynamics of template-directed copolymerization*, J. Stat. Mech.: Th. Exp. 024003 (2017).

[43] T. W. Traut, *Physiological concentrations of purines and pyrimidines*, Mol. Cell. Biochem. **140**, 1–22 (1994).

[44] R. Bernander and A. Poplawski, *Cell Cycle Characteristics of Thermophilic Archaea*, J. Bacteriol. **179**, 4963–4969 (1997).

[45] M. Lundgren, L. Malandrin, S. Eriksson, H. Huber, and R. Bernander, *Cell Cycle Characteristics of Crenarchaeota: Unity among Diversity*, J. Bacteriol. **190**, 5362–5367 (2008).

[46] K. D. Rinker and R. M. Kelly, *Growth Physiology of the Hyperthermophilic Archaeon Thermococcus litoralis: Development of a Sulfur-Free Defined Medium, Characterization of an Exopolysaccharide, and Evidence of Biofilm Formation*, Appl. Env. Microbiol. **62**, 4478–4485 (1996).

[47] W. Zhao, X. Zeng, and X. Xiao, *Thermococcus eurythermalis sp. nov., a conditional piezophilic, hyperthermophilic archaeon with a wide temperature range for growth, isolated from an oil-immersed chimney in the Guaymas Basin*, Int. J. Syst. Evol. Microbiol. **65**, 30–35 (2015).

[48] A. Garai, D. Chowdhury, D. Chowdhury, and T. V. Ramakrishnan, *Stochastic kinetics of ribosomes: Single motor properties and collective behavior*, Phys. Rev. E **80**, 011908 (2009).

[49] D. Chowdhury, *Stochastic mechano-chemical kinetics of molecular motors*, Phys. Rep. **529**, 1–197 (2013).

[50] D. Andrieux and P. Gaspard, *Nonequilibrium generation of information in copolymerization processes*, Proc. Natl. Acad. Sci. USA **105**, 9516–9521 (2008).

[51] P. Gaspard, *Kinetics and thermodynamics of exonuclease-deficient DNA polymerases*, Phys. Rev. E **93**, 042419 (2016).

[52] P. Gaspard, *Kinetics and thermodynamics of DNA polymerases with exonuclease proofreading*, Phys. Rev. E **93**, 042420 (2016).

[53] P. Gaspard, *Template-directed growth of copolymers*, Chaos **30**, 043114 (2020).

[54] Y.-S. Song, Y.-G. Shu, X. Zhou, Z.-C. Ou-Yang, and M. Li, *Proofreading of DNA polymerase: a new kinetic model with higher-order terminal effects*, J. Phys.: Condens. Matter **29**, 025101 (2017).

[55] Q.-S. Li, P.-D. Zheng, Y.-G. Shu, Z.-C. Ou-Yang, and M. Li, *Template-specific fidelity of DNA replication with high-order neighbor effects: A first-passage approach*, Phys. Rev. E **100**, 012131 (2019).

[56] Q.-S. Li, Y.-G. Shu, Z.-C. Ou-Yang, and M. Li, *Kinetic assays of DNA polymerase fidelity: A theoretical perspective beyond Michaelis–Menten kinetics*, Phys. Rev. E **104**, 014408 (2021).

[57] B. Qureshi, J. Juritz, J. M. Poulton, A. Beersing-Vasquez, and T. E. Ouldridge, *A universal method for analyzing copolymer growth*, J. Chem. Phys. **158**, 104906 (2023).

[58] J. E. B. Gunter, B. J. Qureshi, and T. E. Ouldridge, *The interplay of heterogeneity and product detachment in templated polymer copying*, J. Chem. Phys. **162**, 055103 (2025).

[59] N. G. van Kampen, *Stochastic Processes in Physics and Chemistry* (North-Holland, Amsterdam, 1981).

[60] P. Schuster, *Stochasticity in Processes: Fundamentals and Applications to Chemistry and Biology* (Springer International Publishing, Switzerland, 2016).

[61] T. Yasukawa, A. Reyes, T. J. Cluett, M.-Y. Yang, M. Bowmaker, H. T. Jacobs, and I. J. Holt, *Replication of vertebrate mitochondrial DNA entails transient ribonucleotide incorporation throughout the lagging strand*, EMBO J. **25**, 5358–5371 (2006).

[62] J. K. Heinonen, *Biological Role of Inorganic Pyrophosphate* (Springer, New York, 2001).